Modeling and Robust Control of Miniaturized Magnetically-Actuated Optical Image Stabilizers*

Alireza Alizadegan[1], Pan Zhao[1], Ryozo Nagamune[1], and Mu Chiao[1]

***Abstract*— This paper proposes an uncertainty modeling and robust controller design method for miniaturized 3 degrees-of-freedom OISs to deal with its product variabilities. A mathematical model of OISs with product variabilities is developed based on finite element analysis of uncertainties specific for this device. μ-synthesis technique is applied to the uncertainty model to design a robust controller, in order to guarantee robust stability of the closed-loop system and optimize tracking performance against product variabilities. The performance of the μ-synthesis controller is compared with conventional nominal controllers using simulations. The μ-synthesis controller successfully stabilizes the closed-loop system for the entire uncertainty region and suppresses hand-shake disturbances more than 30% better then baseline controllers. This improvement can lead to significant enhancement of image blur in mobile phone cameras equipped with this OIS.**

I. INTRODUCTION

Today, the camera is one of the top features of mobile phones in terms of usage and purchase priorities. Resolution of image sensors in mobile phone cameras is improving every day; however, image blur caused by involuntary hand-shake is an obstacle to their impact on image sharpness [1]. *Optical image stabilizer (OIS)* is an actuator that adjusts the lens or the image sensor to compensate for the hand-shake effect.

So far, the majority of the OIS research has been focused on sensor-shifting design. While sensor-shifting OIS can be size- and cost-efficient for large-scale cameras with replaceable lenses, they have miniaturization limitations and accuracy issues due to their time-varying nonlinear dynamics. These limitations have motivated the application of numerous advanced controller design methods such as fuzzy [2], gain-scheduling [3], sliding mode [4]–[6], adaptive [7], and their combinations [8], [9] to increase robustness of the closed-loop system against variations.

To deal with limitations of sensor-shifting OIS, conceptual design of a novel *lens-tilting* OIS for mobile phone cameras has recently been published [10]. This mechanical design is suitable for miniaturization and low-cost fabrication. In addition, it can simultaneously accomplish image stabilization and auto-focus. An observer-based state-feedback controller was designed and validated experimentally; however, experimental validation was performed only on a 1-DOF prototype rather than the original 3-DOF conceptual design. Moreover, the controller was only tested on one prototype rather than multiple prototypes. The 1-DOF prototype used in this work cannot capture full complexity and coupling of dynamics between different DOFs of the original 3-DOF conceptual design. Besides, the controller design approach used in this work ignores variabilities inherent in low-cost fabrication techniques for small-scale devices [11]–[20]. In [21], we considered control of large-scale prototypes of 3-DOF conceptual design against product variabilities.

In this paper, we deal with control of miniaturized 3-DOF OIS as well as product variabilities. To obtain dynamics of 3-DOF OIS with the effect of product variabilities on dynamics, finite element analysis (FEA) is performed on the miniaturized 3-DOF OIS subject to product variabilities. Based on FEA results, a dynamic uncertainty model is developed to represent dynamics of the miniaturized 3-DOF OIS and product variabilities. To deal with the uncertainty model, the μ-synthesis technique [22] is applied to design a dynamic output-feedback controller that guarantees closed-loop stability against variabilities and optimizes the performance of OIS. The effectiveness of the robust controller is evaluated in simulations by uniformly sampling the uncertainty region and analyzing the controller for the sampled models. Performance of the closed-loop systems equipped with the designed robust controller is compared with those with conventional nominal controllers, such as PID, lead-lag, LQR, and H_∞ controllers using real hand-shake data in time-domain evaluations.

The paper is organized as follows: Section II reviews the mechanical design and the general control system configuration of the miniaturized OIS system proposed in [10]. For the reviewed OIS, in Section III, dynamics and variabilities are determined using finite element analysis. Based on the FEA results, details of the developed dynamic uncertainty model are presented in Section IV. The robust controller is designed in Section V based on the developed uncertainty model and formulation of control objectives of the OIS. Finally, simulations and analyses of the closed-loop system equiped with the designed robust controller are reported in Section VI, followed by comparisons with nominal controllers and discussions of the results.

II. MINIATURIZED OPTICAL IMAGE STABILIZER

In this section, we review the mechanical design and the general control system configuration presented in [10].

*This work was supported by the Natural Sciences and Engineering Research Council of Canada (NSERC) and the Institute for Computing, Information and Cognitive Systems (ICICS) at the University of British Columbia.

[1]The authors are with the Department of Mechanical Engineering, The University of British Columbia, Vancouver, BC V6T1Z4, Canada (e-mail: a.r.alizadegan@gmail.com; panzhao0558@gmail.com; nagamune@mech.ubc.ca, muchiao@mech.ubc.ca).

A. Mechanical design

Figure 1 shows a schematic for mechanical design of the miniature OIS presented in [10]. The lens is held by a monolithic flat structure referred to as the *lens-platform*. The lens-platform encompasses a plate supported by four folded beams connected to the base. The folded beams work as linear springs to provide sufficient stiffness. The plate has 3-DOFs: two rotational DOFs about x-axis and y-axis for image stabilization as well as a translational DOF along z-axis for auto-focus. Actuation of 3-DOFs is achieved by four moving-magnet actuators installed in four corners of the device marked by 1–4 located in equal distances from the central axes. Each moving-magnet actuator consists of a pair of coil and magnet. Magnets are attached to the lens platform whereas coils are fixed to the base. Actuation is achieved by forces generated on each magnet in response to the magnetic fields created by the current in its corresponding coil.

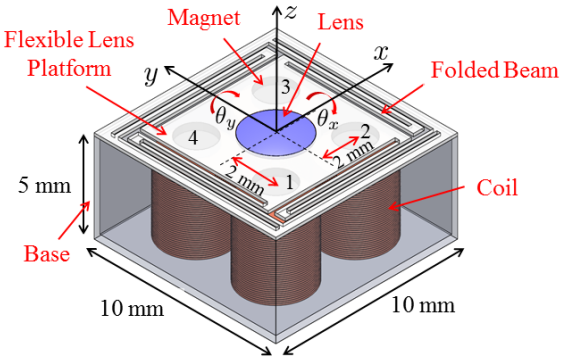

Fig. 1: Mechanical design of the miniature OIS [10]

This conceptual design has pros and cons. The monolithic flat structure of the lens-platform makes it suitable for low-cost MEMS fabrication methods; however, these methods are afflicted by significant product variabilities. These variabilities are significant in the width of the thin folded beams that determines stiffness of the lens-platform. Besides, although using moving-magnet actuators to achieve pure tilt actuation is a low-cost solution, this solution relies on perfect installation and fabrication of eight independent elements (four coils and four magnets). Unavoidable imperfect installation, alignment, and fabrication of coils/magnets (such as number of turns, magnetic strength, equilibrium air-gap, etc.) lead to couplings of shifting dynamics with tilting ones due to force imbalance in an uncertain manner. Finally, hand-shake signals are uncertain in practice, varying from one person to another and from one trial to another for the same person.

In summary, there are three main uncertainties inherent to this conceptual design:

U1) beam width variations in folded beams,
U2) force imbalance in moving-magnet actuators, and
U3) uncertainties in hand-shake disturbance signals.

The uncertainties U1–U3 are to be dealt with the robust controller design method in this paper.

B. General control system configuration

As far as image stabilization is concerned, the OIS's main function is to tilt the lens-platform about either of rotational DOFs to counteract the vibration of the phone body. Since the mechanical design is similar about x- and y-axis, only one of rotational DOFs is considered hereafter. For each rotational DOF, the general control goal is to use the current of individual coils appropriately to tilt the lens-platform to a desired angle according to hand-shake disturbance data supplied by the built-in gyro sensor in the mobile phone. A general feedback control system configuration in Figure 2 was proposed in [10] to achieve this control goal.

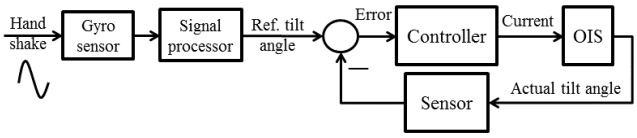

Fig. 2: General control system block-diagram

The hand-shake disturbances are detected by the gyro sensor of the mobile phone and processed to calculate the desired tilt angle of the lens that compensates for the hand-shake disturbances. A negative feedback configuration is used to calculate appropriate current commands to four coils in order to tilt the lens-platform for minimizing the error.

C. Performance specifications and objectives

The performance considerations proposed in this work include four specifications and four objectives. Performance specifications refer to hard constraints that has to be met, while performance objectives refer to performance measures that we wish to improve. Specifications are precedent to objectives, and both are numbered below in descending order of priority. Performance specifications include:

S1) stability of the closed-loop system for all OISs,
S2) maximum of 1% steady-state error to step reference tilt angle in Figure 2,
S3) maximum of 6 dB sensitivity peak to allow sufficient stability margin for modeling errors,
S4) maximum of unity controller gain to avoid input saturation due to noise amplification as well as instability of the closed-loop system due to unmodeled high-frequency dynamics.

After satisfaction of performance specifications, the objectives are:

O1) minimization of the tracking error to improve image blur,
O2) minimization of the control effort to increase battery life, and
O3) reduction of performance degradation against uncertainties U1–U3.

The tracking error is measured by the root mean square (RMS) value of the tracking error signal, while the control effort is assessed by the integral of absolute current values over time.

III. FINITE ELEMENT ANALYSIS

To propose a physics-based dynamic uncertainty model in the next section, a finite element analysis (FEA) is performed in this section to identify dynamics of OIS as well as the effect of uncertainties in beam width and actuator installation on dynamics of OIS. The first and second main modes are associated with the shifting and tilting DOFs, respectively. The eigenfrequencies corresponding to these modes are denoted by ω_{n_s} and ω_{n_t}, respectively.

To identify dynamics of shifting and tilting DOFs, frequency responses of the lens-platform to translational and rotational excitation are obtained. In Figures 3(a) and 3(b), blue solid lines indicate frequency responses of shifting and tilting dynamics obtained from FEA, respectively. The red dashed lines will be explained in the next section. Dynamics are lightly-damped because of its low-friction design.

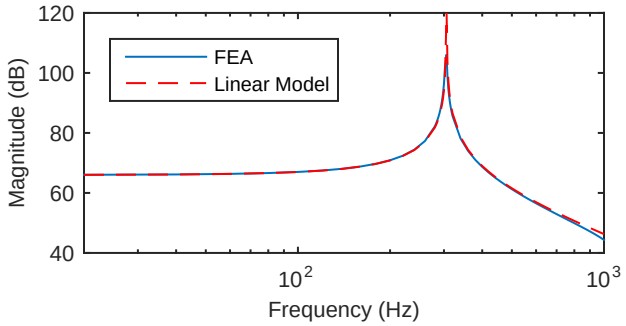

(a) Shifting dynamics

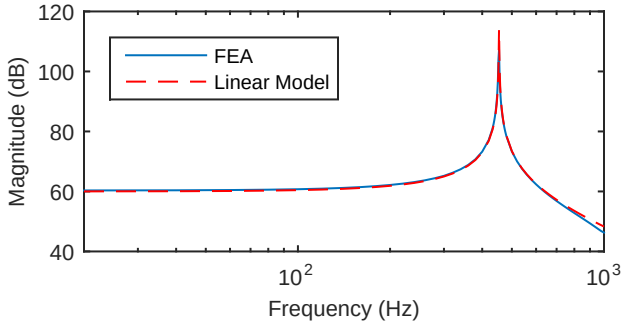

(b) Tilting dynamics

Fig. 3: Nominal dynamics of an OIS

Since the focus in this paper is the tilting, and not the shifting, effects of beam width variation and actuator imbalance are studied on tilting dynamics. Figure 4(a) shows tilting frequency responses of OISs under $\pm 10\%$ beam width variations of the nominal width. Variations in beam width lead to uncertainties in DC gain of tilting dynamics as well as all natural frequencies because the beam width is related to spring stiffness. To be more specific, the increase of beam width increases stiffness, leading to the decrease in DC gain and the increase in natural frequencies. On the other hand, Figure 4(b) displays tilting frequency response of OIS under $\pm 10\%$ imbalance in actuator forces. Force imbalance brings about coupling of shifting dynamics with tilting dynamics.

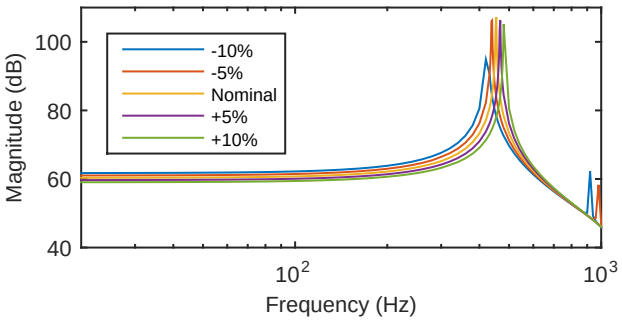

(a) Beam width uncertainties

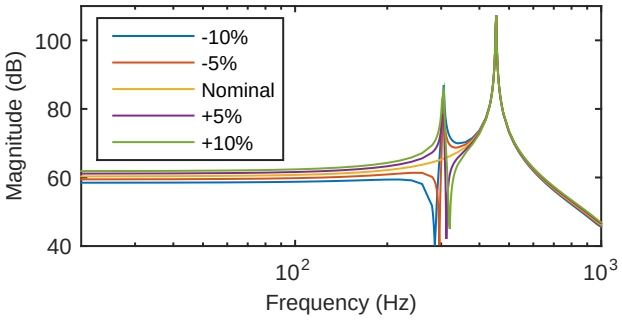

(b) Actuator installation uncertainties

Fig. 4: Effect of uncertainties on tilting dynamics

As the percentage of force imbalance increases, magnitude of coupling increases. The damping ratios do not change in either scenarios because they are affected by material of the lens-platform rather than its geometry.

IV. DYNAMIC UNCERTAINTY MODELING

The objective of dynamic uncertainty modeling is to develop a mathematical representation of the dynamic behavior of the OIS as well as product variabilities based on FEA. The model considers the torque generated on the lens-platform as control input and the tilt angle of the lens-platform as measured output. Based on FEA results, a linear model of the following structure is proposed:

$$G(s,\delta) = G_s(s,\delta) + G_t(s,\delta), \tag{1}$$

where G_s and G_t denote the transfer functions corresponding to the coupling of shift dynamics and tilt dynamics, respectively, and δ designates the uncertainty parameter vector representing product variabilities. For each of these terms, a linear model of the following structure is proposed:

$$G_s(s,\delta) = \frac{K_s\omega_{n_s}^2}{s^2 + 2\xi_s\omega_{n_s}s + \omega_{n_s}^2}, \tag{2}$$

$$G_t(s,\delta) = \frac{K_t\omega_{n_t}^2}{s^2 + 2\xi_t\omega_{n_t}s + \omega_{n_t}^2}, \tag{3}$$

where K, ω_n, and ξ denote respectively DC-gain, natural frequency, and damping ratio.

Based on FEA results, DC-gains as well as all natural frequencies are considered to be uncertain while damping ratios are assumed to be constant for different products. To achieve a control-oriented model, two independent uncertainty parameters are defined as:

$$\delta := [K_s,\ \omega_{n_t}]. \tag{4}$$

Here, K_s is treated as a standalone uncertainty parameter representing force imbalance. Uncertainties in all other uncertain parameters are correlated with uncertainties in ω_{n_t} because they are all due to a common physical source (beam-width variation) as discussed in Section III. The independent uncertainty parameters vary between an upper-bound and a lower-bound as follows:

$$\underline{K_s} < K_s < \overline{K_s}, \quad \underline{\omega_{n_t}} < \omega_{n_t} < \overline{\omega_{n_t}}, \tag{5}$$

where the underline and overline represent respectively the lower-bound and upper-bound of each uncertainty parameter. The upper-bound and lower-bound values should be identified experimentally. The uncertainties in other parameters are correlated with ω_{n_t} using following equations:

$$\omega_{n_s} = \omega^*_{n_s}\omega_{n_t}/\omega^*_{n_t}, \quad K_t = K^*_t(\omega^*_{n_t}/\omega_{n_t})^2, \tag{6}$$

where the superscript * denotes nominal dynamics parameters which should be identified experimentally.

Nominal values for dynamics parameters in (2) and (3) as well as the upper-bound and lower-bound of uncertainty parameters in (5) are identified based on frequency responses in Figure 3 and Figure 4, respectively. Numeric values for nominal natural frequencies and damping ratios of different modes are presented in Table I, while the numeric values for the lower-bound and upper-bound of uncertainty parameters are identified as listed in Table II.

TABLE I: Nominal values of the model parameters

	$K(dB)$	$\omega_n(Hz)$	ξ
G_s	0	306	0.001
G_t	60	453	0.001

TABLE II: Bounds of uncertainty parameters

	Lower-bound	**Upper-bound**
$\omega_{n_t}(Hz)$	428	478
K_s	-259	259

To validate model structure (1), nominal frequency responses of the model G and the FEA model are compared in Figure 3. As shown, the proposed model structure successfully describes dynamics of the system.

Next, to validate uncertainty modeling, samples of frequency responses obtained by varying K_s and ω_{n_t} in the linear model (1) are compared with samples of frequency response obtained by varying force imbalance and beam width in FEA model, respectively. Figures 5(a) and 5(b) are samples of the uncertainty model when ω_{n_t} and K_s are perturbed, respectively. By comparing these samples with Figure 4, it can be seen that variations of K_s and ω_{n_t} represent force imbalance and beam width variation, respectively.

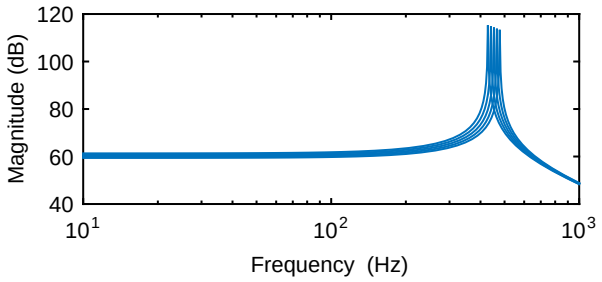

(a) ω_{n_t} uncertainties

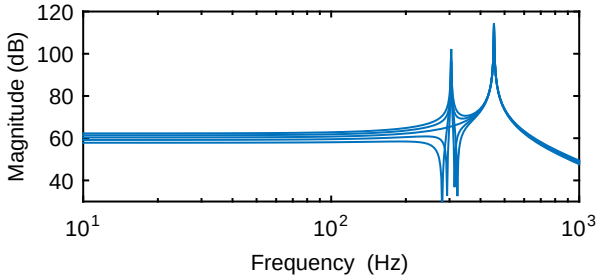

(b) K_s uncertainties

Fig. 5: Effect of uncertainty parameters on frequency responses of model G

V. ROBUST CONTROLLER DESIGN

The μ-synthesis controller design method [22] is applied to the uncertainty model (1). The weighted control system block-diagram used for controller design is shown in Figure 6, where $K(s)$ denotes the dynamic output-feedback robust controller, e is the tracking error, u is the control input (torque), and y is the measured output (tilt angle). r is an uncertain reference signal generated by the hand-shake signal, and δ is the uncertainty parameter vector (4) representing product variabilities.

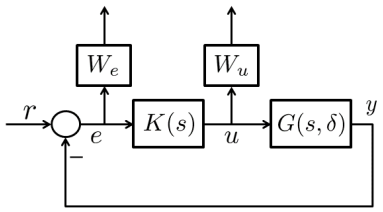

Fig. 6: Weighted control system block-diagram

The robust controller guarantees robust stability (S1) and robust performance (O3) by considering uncertainty parameter δ. The weighting function W_e is used to penalize tracking error (O1), reduce steady-state error (S2), and meet stability margin specifications (S3). On the other hand, W_u is a

weighting function to penalize control effort (O2) and avoid saturation due to noise amplification (S4).

In this paper, a first order W_e parametrization is adopted as:

$$W_e(s) = \frac{s/M_H + \omega_b}{s + \omega_b M_L}, \tag{7}$$

where M_L, M_H, and ω_b are design parameters which, respectively, denote low-frequency gain, high-frequency gain, and bandwidth of W_e^{-1}. To reduce steady state error (S2), M_L should be reduced. Tracking error (O1) can be reduced by increasing ω_b which corresponds to bandwidth. To increase stability margin (S3), sensitivity peak M_H should be reduced. Finally, W_u is taken as a constant gain, and it is increased to reduce control effort (O2) and avoid saturation due to noise amplification (S4). The parameters used for designing the robust H_∞ controller are shown in Table III.

TABLE III: Robust H_∞ controller design parameters

$M_L(dB)$	$\omega_b(Hz)$	$M_H(dB)$	$W_u(dB)$
-40	50	2	100

VI. RESULTS AND DISCUSSIONS

The designed robust controller is compared with four nominal controllers, namely proportional-integral-derivative (PID), lead-lag, linear-quadratic regulator (LQR), and H_∞ controllers. The nominal controllers are designed based on the nominal plant model ($K_s = 0$ and $\omega_{n_t} = 453\ Hz$). The closed-loop system corresponding to different controllers is analyzed for different values of uncertainty parameters in the uncertainty region (5). Figure 7 shows the analysis results. The uncertainty region is illustrated by the red box, and the subregions that are successfully stabilized by different nominal controller design methods are designated by different colors. As shown, none of nominal controllers is capable of stabilizing the closed-loop system for the entire uncertainty region because nominal controller design methods do not take uncertainties into account.

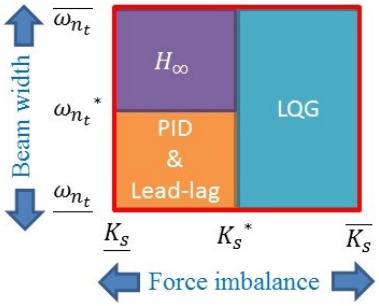

Fig. 7: Closed-loop stability analysis of nominal controllers

Figure 8 shows the results for closed-loop stability analysis of the μ-synthesis controller. In this figure, the green circle and red cross markers, respectively, designate the values of K_s and ω_{n_t} for which the closed-loop system is stable and unstable. As shown, the robust controller design method successfully stabilizes the closed-loop system for assumed uncertainties; furthermore, the μ-synthesis technique systematically optimizes the performance by ensuring robust closed-loop stability only for the uncertainties.

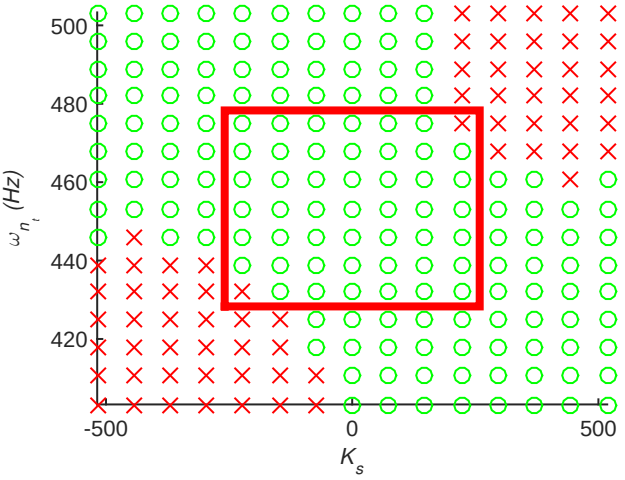

Fig. 8: Closed-loop stability analysis of μ-synthesis

Time-domain performance is assessed by calculating root-mean-square (RMS) values of the tracking error signals. A set of tracking error signals are obtained for three cases corresponding to U1–U3. For each case, mean and standard deviation of RMS values of the corresponding set is calculated. Figure 9 compares time-domain performance of different controllers, where the solid bars and the error bars show the mean values and the standard deviations, respectively. In the figure, nominal controllers are the heuristically de-tuned versions of the controllers in Figure 7 to recover robust stability for uncertainty region 5. Figure 9 demonstrates the robust controller reduces the mean value as well as the standard deviation compared to the nominal controllers because it systematically optimizes the performance by considering uncertainties and utilizing optimization tools in design. More specifically, analysis shows that hand-shake disturbances can be suppressed more than 30% better than nominal controllers.

Figure 10 demonstrates time-domain hand-shake suppression. In this figure, the black solid line is the plot of a real hand-shake signal collected by a mobile phone device. The blue dashed line and red dash-dot line are tracking error signals corresponding to PID controller and μ-synthesis controller. As can be seen, the μ-synthesis controller suppresses hand-shake disturbance more effectively than the PID controller does.

Using the proposed method in practice, a single controller can be designed for the entire product set based on only a small number of product samples. This can save manufacturers time and cost to test, model, and design controller for every single OIS. Moreover, low-cost manufacturing techniques can be employed for fabrication of the lens-platform and assembly of moving-magnet actuators without concern

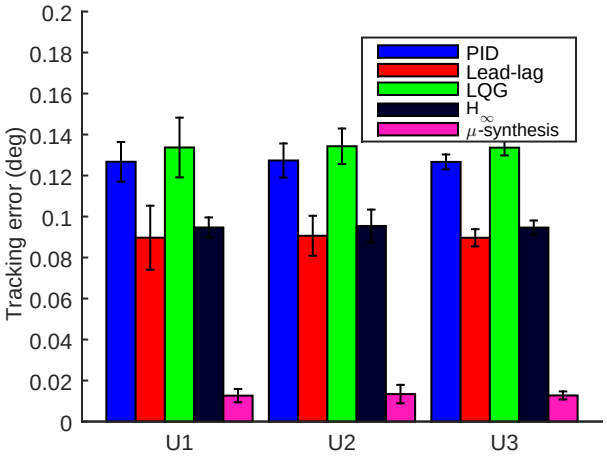

Fig. 9: Time-domain performance of different controllers

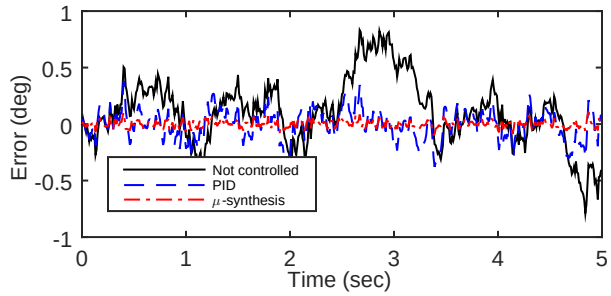

Fig. 10: Comparison of hand-shake disturbance suppression of μ-synthesis with PID in time-domain

about their tolerances. By offering these two benefits, the proposed method leads to less final price, an important factor in mobile phone market.

VII. CONCLUSION

Robust control of miniaturized magnetically-actuated lens-tilting OISs was presented in this paper. A real parametric uncertainty model was developed based on finite element analysis that considers practical product variabilities. A μ-synthesis controller was designed based on the uncertainty model to guarantee closed-loop stability and optimize performance against uncertainties. To evaluate effectiveness of the proposed method, simulations were performed by uniformly sampling the uncertainty region of OIS model. Simulation results demonstrated that the μ-synthesis controller can successfully guarantee closed-loop stability for the entire uncertainty region improve hand-shake suppression more than 30% better than nominal controllers. Finally, practical implications of implementation of the the proposed method on production line of the OIS were discussed. As a future work, the proposed method will be applied to a set of miniaturized OIS prototypes in an experimental setting.

REFERENCES

[1] Q. Hao, X. Cheng, J. Kang, and Y. Jiang, "An image stabilization optical system using deformable freeform mirrors," *Sensors*, vol. 15, no. 1, pp. 1736–1749, 2015.

[2] H. J. Chang, P. J. Kim, D. S. Song, and J. Y. Choi, "Optical image stabilizing system using multirate fuzzy PID controller for mobile device camera," *IEEE Transactions on Consumer Electronics*, vol. 55, no. 2, pp. 303–311, 2009.

[3] D. Yeom, "Optical image stabilizer for digital photographing apparatus," *IEEE Transactions on Consumer Electronics*, vol. 3, no. 55, pp. 1028–1031, 2009.

[4] H.-C. Yu and T. Liu, "Sliding mode control using virtual eigenvalue method for compact optical image stabilization actuators," *IEEE Transactions on Magnetics*, vol. 44, no. 11, pp. 4074–4077, 2008.

[5] R. Palm, "Robust control by fuzzy sliding mode," *Automatica*, vol. 30, no. 9, pp. 1429–1437, 1994.

[6] S. G. Tzafestas and G. G. Rigatos, "A simple robust sliding-mode fuzzy-logic controller of the diagonal type," *Journal of Intelligent and Robotic Systems*, vol. 26, no. 3-4, pp. 353–388, 1999.

[7] H.-C. Yu and T. Liu, "Adaptive model-following control for slim voice coil motor type optical image stabilization actuator," *Journal of Applied Physics*, vol. 103, no. 7, pp. 07F114–1–07F114–3, 2008.

[8] T.-H. S. Li, C.-C. Chen, and Y.-T. Su, "Optical image stabilizing system using fuzzy sliding-mode controller for digital cameras," *IEEE Trans. Consumer Electronics*, vol. 58, no. 2, pp. 237–245, 2012.

[9] T.-H. S. Li and C.-C. Chen, "Extended Kalman filter based hand-shake detector for optical image stabilization using a low cost gyroscope," *IEEE Trans. Consumer Electronics*, vol. 59, no. 1, pp. 113–121, 2013.

[10] P. Pournazari, R. Nagamune, and M. Chiao, "A concept of a magnetically-actuated optical image stabilizer for mobile applications," *IEEE Transactions on Consumer Electronics*, vol. 60, no. 1, pp. 10–17, 2014.

[11] H. G. Harno and R. S. K. Woon, "Robust H_∞ stabilization of a hard disk drive system with a single-stage actuator," in *Proceedings of the IOP Conference Series: Materials Science and Engineering, 2015*, pp. 969–975.

[12] R. Nagamune, X. Huang, and R. Horowitz, "Robust control synthesis techniques for multirate and multisensing track-following servo systems in hard disk drives," *Journal of Dynamic Systems, Measurement, and Control*, vol. 132, no. 2, pp. 021 005–1–021 005–10, 2010.

[13] W. Li and P. X. Liu, "Robust adaptive tracking control of uncertain electrostatic micro-actuators with H_∞ performance," *Mechatronics*, vol. 19, no. 5, pp. 591–597, 2009.

[14] C. Lee and S. M. Salapaka, "Fast robust nanopositioning: A linear-matrix-inequalities-based optimal control approach," *IEEE/ASME Transactions on Mechatronics*, vol. 14, no. 4, pp. 414–422, 2009.

[15] X. Zhang, B. Koo, S. M. Salapaka, J. Dong, and P. M. Ferreira, "Robust control of a mems probing device," *IEEE/ASME Transactions on Mechatronics*, vol. 19, no. 1, pp. 100–108, 2014.

[16] A. Izadbakhsh and S. Rafiei, "Robust control methodologies for optical micro electro mechanical system-new approaches and comparison," in *Proceedings of the Power Electronics and Motion Control Conference, 2008*, pp. 2102–2107.

[17] J. Fei and J. Zhou, "Robust adaptive control of MEMS triaxial gyroscope using fuzzy compensator," *IEEE Transactions on Systems, Man, and Cybernetics, Part B: Cybernetics*, vol. 42, no. 6, pp. 1599–1607, 2012.

[18] E. H. Sarraf, M. Sharma, and E. Cretu, "Novel band-pass sliding mode control for driving MEMS-based resonators," *Sensors and Actuators A: Physical*, vol. 186, pp. 154–162, 2012.

[19] M. Malisoff, F. Mazenc, and M. de Queiroz, "Tracking and robustness analysis for controlled microelectromechanical relays," *International Journal of Robust and Nonlinear Control*, vol. 18, no. 18, pp. 1637–1656, 2008.

[20] M. Shavezipur, K. Ponnambalam, A. Khajepour, and S. Hashemi, "Fabrication uncertainties and yield optimization in MEMS tunable capacitors," *Sensors and Actuators A: Physical*, vol. 147, no. 2, pp. 613–622, 2008.

[21] P. Zhao, A. Alizadegan, R. Nagamune, and M. Chiao, "Robust control of large-scale prototypes for miniaturized optical image stabilizers with product variations," in *Proceedings of the 54th Annual Conference of the Society of Instrument and Control Engineers of Japan (SICE), 2015*, pp. 734–739.

[22] A. Packard and J. Doyle, "The complex structured singular value," *Automatica*, vol. 29, no. 1, pp. 71–109, 1993.